

# 豆壳基炭材料的响应面优化设计及电化学特性

罗路<sup>1</sup>, 邓剑平<sup>1</sup>, 罗凌聪<sup>1</sup>, 陈婷婷<sup>1</sup>, 范毡仔<sup>1,2</sup>, 赵伟刚<sup>1\*</sup>

(1. 福建农林大学材料工程学院, 福州 350018; 2. 英国布鲁内尔大学土木工程学院, 英国 伦敦 UB8 3PH)

**摘要:** 为了满足人们对新型储能设备的需求, 以生物质尤其是农林废弃物基炭材料作为电极材料的超级电容器备受关注。该研究以农业废弃物材料刀豆壳作为前驱体, 采用 KOH 活化方法制备高比面积活性炭并作为超级电容器电极材料。以材料比电容为响应值, 活化温度和活化比例为试验因素, 采用中心复合设计方法 (CCD, Central Composite Design) 进行响应面优化研究, 并探究在最佳工艺条件下制备的活性炭的电化学性能。研究结果表明: 活化温度和活化比例对刀豆壳活性炭材料的比电容均具有显著影响。优化得到的最优工艺参数为活化温度 694 °C, 活化比例 4.17:1。验证试验得到刀豆壳活性炭材料的平均比电容为 254 F/g, 与预测值基本吻合。同时对活性炭进行了性能表征, 采用扫描电镜 (SEM, Scanning Electron Microscope) 和透射电镜 (TEM, Transmission Electron Microscope) 观察活性炭的形貌特征, 通过氮气吸-脱附测试研究了炭材料的孔隙结构, 结果表明: 刀豆壳活性炭材料表面分布大量纳米孔, 最大比表面积可达 3 129 m<sup>2</sup>/g, 总孔隙达 1.68 cm<sup>3</sup>/g, 微孔孔隙达 0.96 cm<sup>3</sup>/g, 有利于电解液流通和电解质离子吸附。

**关键词:** 比表面积; 活性炭; 响应面; KOH 活化; 刀豆壳; 超级电容器

doi: 10.11975/j.issn.1002-6819.2021.10.033

中图分类号: TQ35

文献标志码: A

文章编号: 1002-6819(2021)-10-0277-07

罗路, 邓剑平, 罗凌聪, 等. 豆壳基炭材料的响应面优化设计及电化学特性[J]. 农业工程学报, 2021, 37(10): 277-283.

doi: 10.11975/j.issn.1002-6819.2021.10.033 <http://www.tcsae.org>

Luo Lu, Deng Jianping, Luo Lingcong, et al. Response surface optimization design and electrochemical performance of sword shell-based carbon[J]. Transactions of the Chinese Society of Agricultural Engineering (Transactions of the CSAE), 2021, 37(10): 277-283. (in Chinese with English abstract) doi: 10.11975/j.issn.1002-6819.2021.10.033 <http://www.tcsae.org>

## 0 引言

随着工业的发展和人民生活水平的提高, 对能源的需求也越来越大。近几十年来所使用的能源主要来自储量有限的传统化石燃料, 不可避免地会对环境造成污染<sup>[1]</sup>。因此, 寻找可再生的绿色能源迫在眉睫。同时, 开发可持续能源存储设备也是未来能源储备中不可替代的组成部分<sup>[2]</sup>。

超级电容器是一种介于传统电容器与电池之间的新型储能装置, 因具有充放电速度快、稳定性好、功率密度高和使用寿命长等优势而受到了广泛关注<sup>[3-4]</sup>。超级电容器是生物质能源材料在储能材料领域的重要应用之一<sup>[3]</sup>。经研究表明, 具有大比表面积和孔隙率的活性炭在电解液中吸附离子, 可以在炭材料和电解液的界面上形成电双层<sup>[5]</sup>。为满足新时代对储能材料的需求, 各种各样的生物质和农业废弃物被用作制备超级电容器电极材料的炭前驱体: 豆壳<sup>[6]</sup>、竹子<sup>[7]</sup>、杉木树皮<sup>[8]</sup>、稻壳<sup>[9]</sup>、玉米芯<sup>[10]</sup>等。同时, 杂原子如 B<sup>[11]</sup>, N<sup>[12]</sup>, P<sup>[13]</sup>等可以通过

氧化还原反应提供赝电容, 在炭材料中引入杂原子是提高炭材料比电容的有效方法。因此, 开发具有官能团丰富、比表面积大、孔隙率高的功能炭材料作为超级电容器的优良电极材料具有重要意义。

中国每年产生大量的农业废弃物, 但以刀豆壳作为超级电容器材料前驱体的研究还未见报道。刀豆是豆科植物, 生长较快, 由于其固氮能力<sup>[14]</sup>, 常被用作绿肥和覆盖作物。因此, 刀豆壳不仅是一种性价比高、产量大的农业废弃物, 而且富含氮和氧, 是制备杂原子自掺杂生物质基活性炭的潜在原料。本研究以刀豆壳作为前驱体, 通过 KOH 活化, 合成了具有高度发达的孔隙结构的生物质基活性炭材料。采用响应面法研究活化温度和活化比例与比电容值之间的关系, 建立多元二次回归方程模型来进行拟合分析, 并最终获得最优的工艺参数。

## 1 材料与方法

### 1.1 材料、药品

刀豆壳废弃物作为炭前驱体, 购于湖北省。用自来水清洗刀豆壳去除杂质, 然后将刀豆壳在 50 °C 的鼓风烘箱中放置 3 d 以去除水分, 剪碎备用。

氢氧化钾 (KOH, 85%) 和盐酸 (HCl, 36%~38%), 购自上海阿拉丁生物化学有限公司; 聚偏二氟乙烯 (PVDF, Polyvinylidene Fluoride)、泡沫镍、乙炔黑购于赛博电化学材料网; N-甲基吡咯烷酮 (NMP, N-methylpyrrolidone) 购于天津市致远化学试剂有限公司。

收稿日期: 2021-01-05 修订日期: 2021-04-01

基金项目: 国家自然科学基金资助项目 (31971593); 福建省自然科学基金项目 (高校联合资金) (2019J01386); 福建农林大学科技创新专项基金项目 (CXZZ2019103)

作者简介: 罗路, 博士, 主要从事生物质能源与材料的研究工作。

Email: 75873630@qq.com

\*通信作者: 赵伟刚, 博士, 副教授, 研究领域为生物质基复合材料与多孔炭材料。Email: weigang-zhao@fafu.edu.cn

## 1.2 刀豆壳活性炭的制备

将晒干的刀豆壳剪碎装进瓷坩埚中, 然后将其置于 500 mL/min 氮气环境下的马弗炉, 以 5 °C/min 的升温速率从室温升至 450 °C, 并恒温 1 h。冷却至室温后, 将刀豆壳炭 (Bean shell Charcoal, DC) 研磨粉碎均匀。称取 2 g DC 置于镍坩埚中, 再按碱炭比 (KOH/DC, 下文称活化比例) 为 2、4、6, 称取一定质量的 KOH, 将 KOH 和 DC 混合均匀后置于氮气速率为 500 mL/min 的马弗炉中, 以 3 °C/min 的升温速率从室温升至 600~800 °C 并保持目标温度 2 h。冷却至室温后, 用 1 M HCl 清洗所制得的样品以除去钾离子, 用蒸馏水反复清洗数次直至中性。将获得的刀豆壳基活性炭 DAC 放入鼓风干燥箱中干燥 24 h。所有样品贴上标签 DACx-yy, 其中 x 表示碱炭比 (活化比例), yy 表示活化温度, 例如 DAC4-700 表示活化比例为 4, 活化温度为 700 °C。

## 1.3 刀豆壳基活性炭的微观孔隙及电化学特性测定

### 1.3.1 刀豆壳活性炭的孔结构和表面形貌分析

采用全自动物理吸附仪 (ASAP 2020 HD88, 麦克公司, 美国) 对样品孔隙结构进行表征, 将样品首先于 250 °C 条件下进行脱气 20 h, 然后进行液氮温度下的氮气吸脱附等温线测试, 根据 BET 模型计算活性炭的比表面积 ( $S_{BET}$ ), 通过密度泛函理论 (DFT, Density Functional Theory) 计算活性炭的孔径分布<sup>[15-16]</sup>。利用扫描电镜 (Scanning Electron Microscope, SEM, S-3400, 日立公司, 日本) 和透射电镜 (Transmission Electron Microscope, TEM, JEM-2100UHR, 日本) 分析刀豆壳基活性炭的形貌变化。

### 1.3.2 刀豆壳活性炭的电化学特性

将制备得到的刀豆壳基活性炭材料与乙炔黑、聚偏二氟乙烯 (PVDF, Polyvinylidene Fluoride) 按质量比 8:1:1 混合, 研磨均匀, 加入 N-甲基吡咯烷酮 (NMP, N-methyl Pyrrolidone) 分散剂, 经过超声分散 10 min 得到均匀的浆料, 将浆料涂覆在 1 cm×2 cm 的泡沫镍上, 并置于 85 °C 的烘箱干燥 6 h, 即得到超级电容器工作电极。以 6 mol/L KOH 为电解液组成三电极测试装置用于分析刀豆壳基活性炭材料的各项电化学性能。用 ENNIUM 电化学工作站完成工作电极在三电极体系下的各项测试, 包括恒电流充放电 (GCD, Galvanostatic Charge-Discharge)、循环伏安曲线 (CV, Cyclic Voltammetry) 和交流阻抗特性 (EIS, Electrochemical Impedance Spectroscopy)。其中恒流充放电电势窗口为 -1~0 V, 电流密度为 1~20 A/g; 循环伏安测试电势窗口为 -1~0 V, 扫描速率为 2~100 mV/s; 交流阻抗测试在开路电压 5 mV 下进行, 频率区间为 10 mHz~100 kHz。采用铂片为对电极, 汞-氧化汞电极为参比电极。材料的比电容通过恒流放电曲线计算, 计算公式如下<sup>[17]</sup>:

$$C = I \cdot \Delta t / (m \cdot \Delta V) \quad (1)$$

式中  $C$  是电极的质量比电容, F/g;  $I$  是恒定放电电流, A;  $\Delta t$  是放电时间, s;  $m$  是活性物质的负载量, g;  $\Delta V$  是放电电势窗口, V。

## 1.4 响应面优化试验

以活化温度和活化比例为试验因素, 质量比电容为响应值, 利用软件 Design-Expert 12 进行中心复合设计和响应面分析设计, 选用 2 因素 3 阶  $n=13$  试验, 中心点重

复次数为 5 次 (如表 1 所示)。对所得模型进行方差分析从而确定模型和回归系数的显著性。同时对优化后的工艺参数进行试验验证。

表 1 响应面分析的因素水平表

| 水平<br>Levels | 活化比例<br>Activation ratio $A$ | 活化温度<br>Activation temperature $B/^\circ\text{C}$ |
|--------------|------------------------------|---|
| -1           | 2                            | 600   |
| 0            | 4                            | 700   |
| 1            | 6                            | 800   |

## 2 结果与分析

### 2.1 活性炭结构表征和形貌分析

图 1a 所示为刀豆壳基多孔炭材料的氮气吸脱附曲线, 在相对压力非常低时 ( $P/P_0 < 0.05$ ),  $N_2$  吸附量急剧增加; 随着压力升高,  $N_2$  吸附趋势趋于平缓, 没有吸附-脱附滞后回环。根据 IUPAC 分类, 刀豆壳基活性炭材料的  $N_2$  吸附-脱附等温线为 I 型, 说明炭材料中存在大量微孔<sup>[18]</sup>。众所周知, 不同的前驱体对材料最终的孔隙结构具有决定性的影响, 同时也将影响其制备工艺参数的选择和优化<sup>[19-20]</sup>。根据 BET 模型计算炭材料的比表面积, 最高可达 3 129  $\text{m}^2/\text{g}$ , 最大孔径可达 1.68  $\text{cm}^3/\text{g}$ , 详细的孔隙结构参数如表 2 所示。从表 2 可以看出, 炭材料的比表面积随着活化温度和活化比例的升高而增大, 同时总孔容也有相似的趋势。这是由于增加活化剂并提高活化温度, 可以促进造孔和扩孔作用, 使比表面积, 孔容和平均孔径增大。同时, 扩孔作用使微孔数量不断减小, 但所有样品的微孔比例都保持在 50% 以上。图 1b 显示了样品的孔径分布曲线, 不同温度的炭材料具有相似的孔径分布曲线。从图 1b 可以看出, 刀豆壳基活性炭材料的孔径主要分布在 0.5 nm 到 4 nm 之间, 同时存在微孔和孔径较小的介孔, 有利于电解质离子的传输和吸附<sup>[19-20]</sup>。

表 2 样品的孔结构参数

| 样品<br>Samples | 比表面积<br>Specific surface area<br>$S_{BET}/(\text{m}^2 \cdot \text{g}^{-1})$ | 总孔容<br>Total volume<br>$/(\text{cm}^3 \cdot \text{g}^{-1})$ | 微孔孔容<br>Micropore volume<br>$/(\text{cm}^3 \cdot \text{g}^{-1})$ | 介孔孔容<br>Mesopore volume<br>$/(\text{cm}^3 \cdot \text{g}^{-1})$ | 微孔比例<br>Mesopore ratio | 平均孔径<br>Average pore size/nm |
|---------------|---|---|--|---|------------------------|------------------------------|
| DAC2-600      | 1 436   | 0.64  | 0.61   | 0.03  | 0.96                   | 0.93                         |
| DAC4-600      | 2 027   | 0.87  | 0.78   | 0.09  | 0.89                   | 1.26                         |
| DAC6-600      | 1 624   | 0.77  | 0.62   | 0.15  | 0.81                   | 1.45                         |
| DAC2-700      | 1 868   | 0.95  | 0.71   | 0.24  | 0.75                   | 1.45                         |
| DAC4-700      | 2 282   | 1.12  | 0.72   | 0.40  | 0.64                   | 1.61                         |
| DAC6-700      | 3 129   | 1.68  | 0.96   | 0.72  | 0.57                   | 1.94                         |
| DAC2-800      | 1 537   | 0.79  | 0.59   | 0.20  | 0.75                   | 1.18                         |
| DAC4-800      | 2 072   | 1.50  | 0.85   | 0.65  | 0.57                   | 1.73                         |
| DAC6-800      | 2 836   | 1.54  | 0.84   | 0.70  | 0.55                   | 1.79                         |

注: DACx-yy, 其中 x 表示碱炭比 (活化比例), yy 表示活化温度, 下同。  
Note: DACx-yy, where x represents alkali-carbon ratio (activation ratio) and yy represents activation temperature, the same below.

利用扫描电镜观察刀豆壳基炭材料 DAC4-700 的表面形貌, 如图 2a 所示, 刀豆壳基炭材料表面上有许多孔, 大孔壁上形成小孔, 开孔率高, 孔与孔之间相互连通, 这有助于电解质离子的传输, 同时能使电解质离子很好

的扩散进入到内部微孔中，提高微孔利用率<sup>[21]</sup>。为了进一步研究刀豆壳基炭材料的形态，使用透射电镜观察孔结构，如图 2b 所示。从图 2b 中可以观察到大量的纳米孔，这与 SEM 与氮气的吸脱附结果一致。

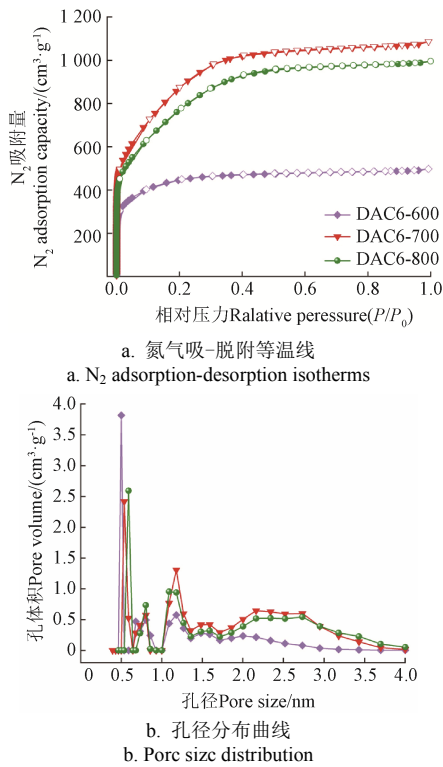
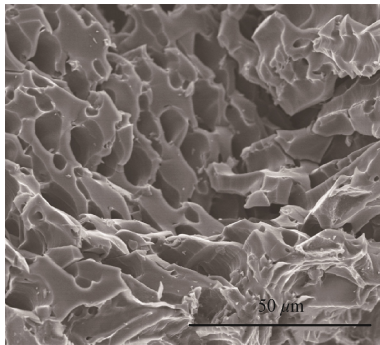
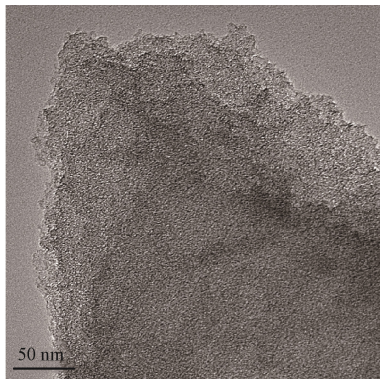


图 1 刀豆壳活性炭的 N<sub>2</sub>-吸脱附等温线和孔径分布曲线  
Fig.1 N<sub>2</sub> adsorption-desorption isotherms and pore size distribution of activated carbon from sword shells



a. DAC4-700 的扫描电镜图  
a. Scanning Electron Microscope (SEM) image of DAC4-700



b. DAC4-700 的透射电镜图  
b. Transmission Electron Microscope (TEM) image of DAC4-700

图 2 刀豆壳活性炭的扫描电镜和透射电镜结果

Fig.2 SEM and TEM images of activated carbon from sword shells

## 2.2 响应面试验设计与结果

基于表 1 的试验设计，由 Design-Expert 12 设计得到的具体的试验设计方案见表 3。以活化温度，活化比例为试验因素，以电流密度 1 A/g 条件下的质量比电容为响应值，对其进行拟合并建立二次方程式的回归模型，其模型为

$$Y = -3148.48851 + 160.06178A + 8.85224B + 0.02625AB - 21.38793A^2 - 0.006455B^2 \quad (2)$$

对其进行方差分析，结果如表 4 所示。模型  $F$  值为 65.06，概率  $P$  值小于 0.0001，表示本试验所选取的模型显著性极好，说明此方法可信度较高，对真实的两因素三水平试验用该模拟方程来描述是可行的。同时，该二次多项式回归模型中， $A^2$  和  $B^2$  的  $P$  值小于 0.0001，说明这 2 项对刀豆壳活性炭比电容的响应值影响极显著。模型的校正决定系数  $R^2=97.54\%$ ，修正系数为 95.78%，均大于 95%，表明线性关系良好，说明使用该模型可以较好的预测刀豆壳基活性炭的比电容值，且预测值与实测值之间的相关性非常高，试验过程中的误差极小<sup>[22-23]</sup>。需要指出的是，失拟值可以评估模型的拟合度，对于刀豆壳基活性炭比电容的回归方程模型， $P$  值为 0.075，大于 0.05 的水平，说明模型失拟不显著，证明该模型与数据拟合度良好。

表 3 CCD 试验设计及结果

Table 3 Experimental design and results of CCD

| 序号<br>No. | 活化比例<br>Activation ratio $A$ | 活化温度<br>Activation temperature $B/^\circ\text{C}$ | 比电容<br>Specific capacitance/ $(\text{F}\cdot\text{g}^{-1})$ |
|-----------|------------------------------|---|---|
| 1         | 2                            | 700   | 149   |
| 2         | 6                            | 600   | 120   |
| 3         | 4                            | 800   | 161   |
| 4         | 2                            | 600   | 101   |
| 5         | 4                            | 700   | 264   |
| 6         | 4                            | 600   | 208   |
| 7         | 4                            | 700   | 270   |
| 8         | 4                            | 700   | 260   |
| 9         | 4                            | 700   | 268   |
| 10        | 4                            | 700   | 256   |
| 11        | 6                            | 700   | 178   |
| 12        | 2                            | 800   | 90  |
| 13        | 6                            | 800   | 130   |

活化比例与活化温度对比电容的响应面结果如图 3 所示，刀豆壳基活性炭的比电容随着活化比例和活化温度的升高而增加。当活化比例固定时，比电容随着活化温度的升高先上升后下降，在 700℃ 左右达到峰值，随着活化温度的进一步升高，比电容呈现下降的趋势。这是因为在高温条件下 KOH 能有效地与刀豆壳中的碳进行反应，使物料内部不断发生开孔和扩孔，最终形成具有发达孔隙结构的活性炭<sup>[24-25]</sup>。但是当活化温度过高时，碳骨架遭到过渡刻蚀，微孔不断向中孔和大孔转变，同时会导致部分孔隙坍塌破坏，不利于电解液离子的吸附，从而导致比电容的降低<sup>[26]</sup>。当反应温度固定时，比电容随着活化比例的增大先增大后趋于缓和。在活化比例为 4 时，比电容达到最大值。当活化比例进一步增大，活性炭烧失率也随之增大，样品得率下降明显，同时炭骨架

内部孔隙结构发展到一定程度后,由原来孔的加深变为孔的拓宽,使一部分微孔转化成中孔和大孔,从而降低

了炭材料的比表面积,同时减少了炭材料对电解液离子的吸附位点数量,导致比电容降低<sup>[12]</sup>。

表4 活性炭比电容的回归方程方差分析

Table 4 Analysis of variance of the regression equation of activated carbon specific capacitance

| 方差来源 Source of variance | 平方和 Sum of squares | 自由度 Degree of freedom | 均方 Mean square | F值 F value | P值 P value | 显著性 Significant |
|-------------------------|--------------------|-----------------------|----------------|------------|------------|-----------------|
| 模型 Model                | 52 487.48          | 5                     | 10 497.50      | 55.45      | < 0.000 1  | ***             |
| A                       | 1 290.67           | 1                     | 1 290.67       | 6.82       | 0.034 9    | *               |
| B                       | 384.00             | 1                     | 384.00         | 2.03       | 0.197 5    |                 |
| AB                      | 110.25             | 1                     | 110.25         | 0.582 3    | 0.470 3    |                 |
| A <sup>2</sup>          | 20 214.65          | 1                     | 20 214.65      | 106.77     | < 0.000 1  | ***             |
| B <sup>2</sup>          | 11 508.65          | 1                     | 11 508.65      | 60.79      | 0.000 1    | ***             |
| 残差 Residual             | 1 325.29           | 7                     | 189.33         |            |            |                 |
| 失拟项 Lack of fit         | 1 050.09           | 3                     | 350.03         | 5.09       | 0.075      |                 |
| 纯误差 Pure error          | 275.20             | 4                     | 68.80          |            |            |                 |
| 总变异 Total               | 53 812.77          | 12                    |                |            |            |                 |

注:显著性检验采用最小显著差法:\*差异显著, $P < 0.05$ ,\*\*差异高度显著, $P < 0.01$ ,\*\*\*差异极显著, $P < 0.001$ 。

Note: The significance test was performed using the minimum significant difference method: \* significant difference,  $P < 0.05$ , \*\* highly significant difference,  $P < 0.01$ , \*\*\* very significant difference,  $P < 0.001$ .

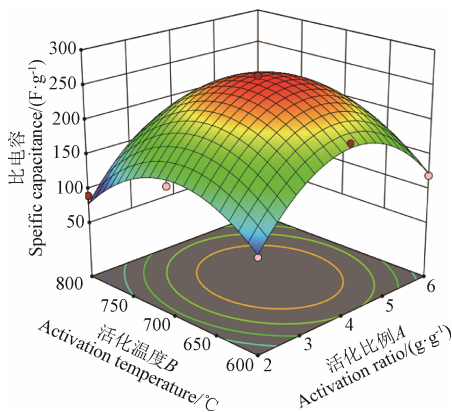


图3 活性炭比电容的响应面图及其相应的等高线图

Fig.3 The response surface diagram of activated carbon specific capacitance and its corresponding contour map

将表2中材料的孔隙结构和表3中材料比电容的数据进行分析可知,材料的比电容虽然会受孔隙结构的影响,但是二者之间却没有明显的线性关系,是受比表面积、孔容大小和孔径分布等多因素的共同影响和作用<sup>[8]</sup>。Hao等人报道指出,多孔材料中,只有尺寸接近电解质离子的尺寸的孔径能发挥出材料的最佳性能<sup>[27]</sup>。同时还需要指出的是,刀豆壳作为活性炭材料制备的前驱体,其含有较为丰富的氮、氧等杂原子,所以经过不同的活化温度和活化比例处理后,材料最终的杂原子含量也会影响材料最终的比电容大小,所以关于材料的电化学特性与孔隙结构以及杂原子含量之间的定量的研究还需进一步的探究,这也将是炭材料作为超级电容器电极材料研究的重点。

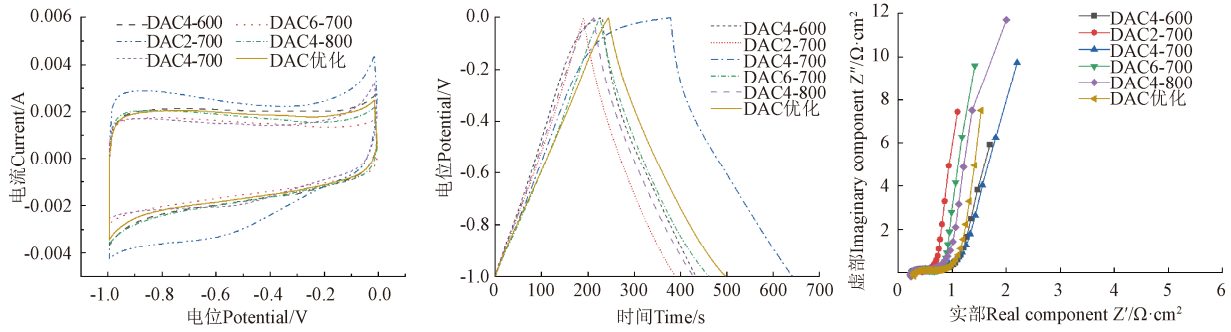
### 2.3 工艺参数优化与模型试验

通过上述方程对刀豆壳基活性炭的比电容值进行预测,优化得到的最佳活性炭制备条件为:活化温度694℃,活化比例4.17。在此制备条件下,预测的比电容值为261 F/g。为了验证模型和响应面分析试验数据的准确性和可靠性,采用优化的制备工艺进行试验,其实际的比电容值见表5。进行3次平行试验取平均值,得到刀豆壳

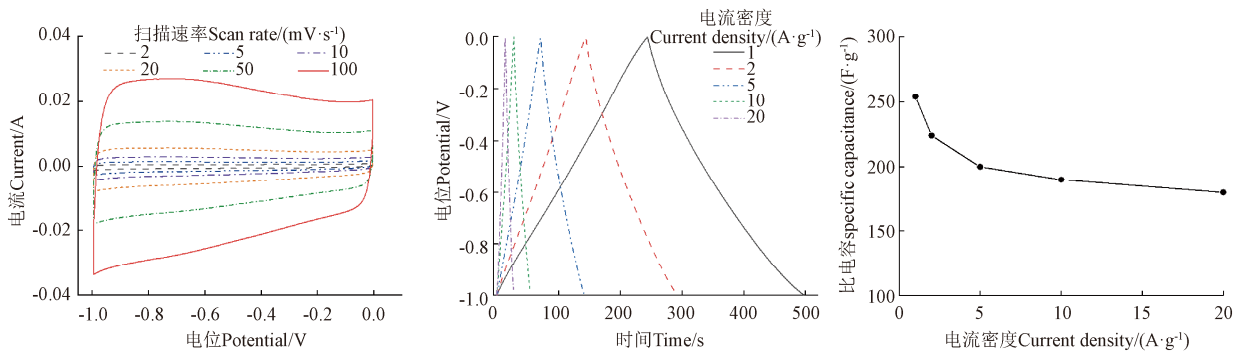
活性炭的比电容为254 F/g,与预测值相差仅2.68%,可知试验结果与预测值相符,该模型预测结果可靠。表5优化工艺条件下制备的刀豆壳基活性炭的循环伏安曲线(CV),恒流充放电曲线(GCD)和交流阻抗曲线(Electrochemical Impedance Spectroscopy, EIS)分别如图4a、4b和4c所示,同时为了便于比较,分别加入了不同的活化温度和活化比例的刀豆壳基活性炭作为比较。从图4a和4b可以观察到,不同条件下制备的刀豆壳基活性炭和优化后的活性炭的CV和GCD曲线形状相似且分别呈现出准矩形和偏离线性的近三角形形状,均表现出良好的电容性能。图4c显示了不同样品的交流阻抗曲线图,在低频区近似垂直的斜线表明电极/电解液界面良好的离子扩散能力<sup>[28-29]</sup>。从图中可以看出,不同样品的斜率相近,表明样品都具有较好的离子扩散能力。高频区轴截距与电极材料的内阻( $R_s$ )有关,从图中可以看出,所有样品的内阻都很低( $< 1 \Omega$ ),说明不同的制备工艺条件下制得的样品均具有良好的电子导电性<sup>[30]</sup>。图4d显示了优化的活性炭在不同扫描速率下的CV曲线,从图中可以看出, CV曲线拥有良好的对称性并呈类矩形,表明样品具有良好的双电层电容特性;当扫描速率从2 mV/s增大到100 mV/s时, CV曲线仍能保持良好的对称性和类矩形形状,表明其具有快速的离子响应速率以及良好的倍率性能。图4e显示了优化的刀豆壳基活性炭在不同电流密度下的GCD曲线,从图中可以看出, GCD曲线不存在明显电压降,表明炭材料具有较小的内部电阻。同时,不同的电流密度下的GCD曲线均呈现良好的对称性和线性,表明刀豆壳基活性炭具有良好的电化学可逆性<sup>[31]</sup>。图4f所示为优化的活性炭在不同电流密度下的质量比电容值,在1 A/g时的最大比电容为254 F/g,当电流密度增大到20 A/g时,其比电容保持率高达70.8%,倍率性能优异。将此优化的活性炭的比电容结果与公开发表的文献进行比较,见表6,可以发现,刀豆壳基活性炭表现出了非常优异的电化学性能,其质量比电容明显较高。同时对比也可发现,纳米炭材料作为超级电容器的电极材料,其比电容值的大小并未随着比

表面积的增大而增大，二者之间没有必然的线型关系。刀豆壳基活性炭良好的电化学性能不仅来自于其较大

的比表面积和孔容大小，更与其孔径大小和分布等密切相关<sup>[6-7]</sup>。



a. 刀豆壳活性炭在  $5 \text{ mV}\cdot\text{s}^{-1}$  下的循环伏安曲线  
 a. CV curves of sword shell based activated carbon at  $5 \text{ mV}\cdot\text{s}^{-1}$   
 b. GCD curves of sword shell-based activated carbon at  $1 \text{ A}\cdot\text{g}^{-1}$   
 c. 豆壳活性炭的交流阻抗曲线  
 c. EIS curves of sword shell-based activated carbon



d. 优化后的活性炭在不同扫描速率下的循环伏安曲线  
 d. CV curves of optimized activated carbon at different scan rate  
 e. 优化后的活性炭在不同电流密度下的恒流充放电曲线  
 e. GCD curves of optimized activated carbon at different current density  
 f. 优化后的活性炭在不同电流密度下的比电容  
 f. Specific capacitance of optimized activated carbon at different current density

图 4 三电极系统刀豆壳活性炭的电化学性能测试

Fig.4 Electrochemical performance characteristics measured in a three-electrode system

表 5 刀豆壳活性炭的工艺参数优化和试验验证结果

Table 5 Optimization of process parameters and experimental verification results of sword shell activated carbon

| 序号<br>Numbers | 活化比例<br>Activation ratio A | 活化温度<br>Activation temperature B/°C | 比电容 Specific capacitance/(F·g <sup>-1</sup> ) |                            |
|---------------|----------------------------|-------------------------------------|---|----------------------------|
|               |                            |                                     | 预测值<br>Predicted values                       | 试验值<br>Experimental values |
| 1             |                            |                                     |   | 253                        |
| 2             | 4.17                       | 694                                 | 261   | 260                        |
| 3             |                            |                                     |   | 249                        |

表 6 刀豆壳活性炭的电容性能与文献报道的比较

Table 6 Comparison of electrochemical performance with the reported literatures

| 样品<br>Samples           | 比表面积<br>Specific surface area/(m <sup>2</sup> ·g <sup>-1</sup> ) | 电流密度<br>Current density/(A·g <sup>-1</sup> ) | 比电容<br>Specific capacitance/(F·g <sup>-1</sup> ) | 参考文献<br>References |
|-------------------------|--|--|--|--------------------|
| 刀豆壳基活性炭 (DAC 优化)        | 2 452  | 1  | 254  | 本研究                |
| 杉木皮基活性炭(BNC-20)         | 891  | 0.5  | 188  | [8]                |
| 毛豆壳基活性炭 (MHT-20min-10%) | 994  | 0.2  | 120  | [32]               |
| 稻壳基活性炭 (RHPC)           | 527  | 0.1  | 110  | [33]               |
| 泡沫基活性炭 (PC)             | 620  | 1  | 208  | [34]               |
| 大麻基活性炭 (Hurd-a-5)       | 2 801  | 1  | 167  | [35]               |
| 煤衍生炭(BNAC-850)          | 1 288  | 0.5  | 176  | [36]               |
| 香蒲基活性炭(CAC)             | 441  | 0.5 <sup>1</sup>                             | 127  | [37]               |

### 3 结 论

1) 以农业废弃物刀豆壳为前驱体，采用低温炭化和 KOH 高温活化两步法，成功制备了具有高比表面积和孔容的活性炭并应用于超级电容器电极材料。

2) 通过 SEM 和 TEM 分析刀豆壳基活性炭的微观形貌，发现活性炭表面分布着大量相互连通的孔隙结构，开孔率高。通过氮气吸-脱附测试活性炭的孔隙结构，结果表明其最大比表面积可达  $3\ 129 \text{ m}^2/\text{g}$ ，总孔容达  $1.68 \text{ cm}^3/\text{g}$ ，微孔孔容可达  $0.96 \text{ cm}^3/\text{g}$ ，有利于电解质离子的传输和吸附。

3) 通过响应面分析活化温度和活化比例对电极材料比电容的影响。由分析结果可知：活化温度和活化时间对电极材料比电容均具有显著影响。通过对模型进行拟合建立二元回归方程，进而优化得到最佳活性炭制备条件，即在活化温度  $694 \text{ }^\circ\text{C}$ ，活化比例  $4.17:1$  条件下制备的刀豆壳基活性炭材料理论比电容可达到  $261 \text{ F/g}$ 。验证试验得到的平均比电容为  $254 \text{ F/g}$ ，与预测值基本吻合。

4) 以刀豆壳作为超级电容器电极材料，其电化学性能接近于甚至高于大部分的多孔炭材料。本研究也同时发现，炭材料的电化学性能虽然与材料的孔隙结构密切相关，但是并没有必然的线性关系，关于炭材料的微观结构与电容特性的定量关系还有待进一步探究。

## [参 考 文 献]

- [1] Chee W K, Lim H N, Zainal Z, et al. Flexible graphene-based supercapacitors: A review[J]. *Journal of Physical Chemistry C*, 2016, 120: 4153-4172.
- [2] Chu M, Zhai Y, Shang N, et al. N-doped carbon derived from the monomer of chitin for high-performance supercapacitor[J]. *Applied Surface Science*, 2020, 517: 146140.
- [3] 韩尊强, 钟伟婷, 王堃. 氮掺杂竹炭基超级电容器电极材料制备与表征[J]. *林业工程学报*, 2020, 5(5): 76-83. Han Zunqiang, Zhong Weiting, Wang Kun. Preparation and characterization of nitrogen-doped bamboo charcoal supercapacitor electrode materials[J]. *Journal of Forestry Engineering*, 2020, 5(5): 76-83. (in Chinese with English abstract)
- [4] 左宋林, 王永芳, 张秋红. 活性炭作为电能储存和能源转化材料的研究进展[J]. *林业工程学报*, 2018, 3(4): 1-11. Zuo Songlin, Wang Yongfang, Zhang Qiuhong. Activated carbon for the electrochemical storage of energy and electrochemical catalytic conversion of fuels: A review[J]. *Journal of Forestry Engineering*, 2018, 3(4): 1-11. (in Chinese with English abstract)
- [5] Wang L, Gao Z, Chang J, et al. Nitrogen-doped porous carbons as electrode materials for high-performance supercapacitor and dyesensitized solar cell[J]. *ACS Applied Materials & Interfaces*, 2015, 7: 20234-20244.
- [6] Chen T, Luo L, Li Z, et al. Preparation and characterization of nitrogen and oxygen heteroatom codoped activated biocarbons from edamame shell[J]. *BioResources*, 2018, 13(2): 3932-3948.
- [7] Chen T, Zhou Y, Luo L, et al. Preparation and characterization of heteroatom self-doped activated biocarbons as hydrogen storage and supercapacitor electrode materials[J]. *Electrochimica Acta*, 2019, 325: 134941.
- [8] Luo L, Zhou Y, Yan W, et al. Two-step synthesis of B and N co-doped porous carbon composites by microwave-assisted hydrothermal and pyrolysis process for supercapacitor application[J]. *Electrochimica Acta*, 2020, 360: 137010.
- [9] 肖程元, 张文礼, 林海波, 等. 稻壳基活性炭的热处理改性及其电化学性能[J]. *新型炭材料*, 2019, 34(4): 341-348. Xiao Chengyuan, Zhang Wenli, Lin Haibo, et al. Modification of a rice husk-based activated carbon by thermal treatment and its effect on its electrochemical performance as a supercapacitor electrode[J]. *New Carbon Material*, 2019, 34(4): 341-348. (in Chinese with English abstract)
- [10] 邢宝林, 陈丽薇, 张传祥, 等. 玉米芯活性炭的制备及其电化学性能研究[J]. *材料导报*, 2015, 29(3): 45-48. Xing Baolin, Chen Wei, Zhang Chanxiang, et al. Preparation and electrochemical performance of corncob-based activated carbon[J]. *Materials Reports*, 2015, 29(3): 45-48. (in Chinese with English abstract)
- [11] Ling Z, Wang Z, Zhang M, et al. Sustainable synthesis and assembly of biomass-derived B/N co-doped carbon nanosheets with ultrahigh aspect ratio for high-performance supercapacitors[J]. *Advanced Functional Materials*, 2016, 26: 111-119.
- [12] Niu Q, Zhao S, Gao K, et al. Natural nanofibers stacked porous nitrogen-doped carbon nanosheets with promising capacitive performance[J]. *Cellulose*, 2019, 26: 5395-5407.
- [13] Zhang H, Zhang C, Zhang Y, et al. P/N codoped carbon derived from cellulose: A metal-free photothermal catalyst for transfer hydrogenation of nitroarenes[J]. *Applied Surface Science*, 2019, 487: 616-624.
- [14] Adebawale K O, Afolabi T A, Olu-owolabi B I. Functional, physicochemical and retrogradation properties of sword bean (*Canavalia gladiata*) acetylated and oxidized starches[J]. *Carbohydrate Polymers*, 2006, 65: 93-101.
- [15] Brunauer S, Emmet P H, Teller E. Adsorption of gases in multimolecular layers[J]. *Journal of the American Chemical Society*, 1938, 60(2): 309-319.
- [16] Tarazona P. Solid-fluid transition and interfaces with density functional approaches[J]. *Surface Science*, 1995, 331: 989-994.
- [17] Zhao Z C, Xie Y B. Electrochemical supercapacitor performance of boron and nitrogen co-doped porous carbon nanowires[J]. *Journal of Power Sources*, 2018, 400: 264-276.
- [18] Lia J, Xie L, Xiong D, et al. Enhanced capacitance of boron-doped graphene aerogels for aqueous symmetric supercapacitors[J]. *Applied Surface Science*, 2019, 475: 285-293.
- [19] 李大伟, 田原宇, 郝俊辉, 等. 炭活化一步法制备豆渣基极微孔活性炭[J]. *农业工程学报*, 2015, 31(19): 309-314. Li Dawei, Tian Yuanyu, Hao Junhui, et al. Preparation of N-doped ultramicropore-containing active carbons from waste soybean dreg by one-step carbonization/activation[J]. *Transactions of the Chinese Society of Agricultural Engineering (Transactions of the CSAE)*, 2015, 31(19): 309-314. (in Chinese with English abstract)
- [20] 牛文娟, 冯雨欣, 钟菲, 等. 秸秆微波水热炭和活性炭理化及电化学特性[J]. *农业工程学报*, 2020, 36(17): 202-212. Niu Wenjuan, Feng Yuxin, Zhong Fei, et al. Physicochemical and electrochemical properties of microwave-assisted hydrochars and activated carbons from straws[J]. *Transactions of the Chinese Society of Agricultural Engineering (Transactions of the CSAE)*, 2020, 36(17): 202-212. (in Chinese with English abstract)
- [21] Li Y, Wang G, Wei T, et al. Nitrogen and sulfur co-doped porous carbon nanosheets derived from willow catkin for supercapacitors[J]. *Nano Energy*, 2016, 19: 165-175.
- [22] 陈俊英, 冯向应, 史召霞, 等. 响应面法优化混合活化剂制备脱硅稻壳基活性炭[J]. *郑州大学学报*, 2015, 36(2): 120-124. Chen Junying, Feng Xiangying, Shi Zhaoxia, et al. Optimization of activated carbon preparation from desilicon rice husk via compound agents by response surface methodology[J]. *Journal of Zhengzhou University*, 2015, 36(2): 120-124. (in Chinese with English abstract)
- [23] Huang Y P, Hou C H, Shi H C, et al. Optimization of highly microporous activated carbon preparation from Moso bamboo using central composite design approach[J]. *Journal of the Taiwan Institute of Chemical Engineers*, 2015, 50: 266-275.
- [24] Zhao W, Fierro V, Zlotea C, et al. Optimization of activated carbons for hydrogen storage[J]. *International Journal of Hydrogen Energy*, 2011, 36(18): 11746-11751.
- [25] Zhao W, Fan M, Gao H, et al. Central composite design approach towards optimization of super activated carbons from bamboo for hydrogen storage[J]. *RSC Advance*, 2016, 6(52): 46977-46983.
- [26] Raj C J, Rajesh M, Manikandan R, et al. High electrochemical capacitor performance of oxygen and nitrogen enriched activated carbon derived from the pyrolysis and activation of squid gladius chitin[J]. *Journal of Power Sources*, 2018, 386: 66-76.
- [27] Hao L, Li X, Zhi L. Carbonaceous electrode materials for supercapacitors[J]. *Advanced Materials*, 2013, 25(28): 3899-3904.
- [28] Wan L, Xiao R, Liu J, et al. A novel strategy to prepare N, S-codoped porous carbons derived from barley with high surface area for supercapacitors[J]. *Applied Surface Science*,

- 2020, 518: 146265.
- [29] Shi C, Hua L, Hou J, et al. Alkali metal boosted atom rearrangement in amorphous carbon towards crystalline graphitic belt skeleton for high performance supercapacitors[J]. *Energy Storage Materials*, 2018, 15: 82-90.
- [30] Ma Y, Zhang X, Liang Z, et al. B/P/N/O co-doped hierarchical porous carbon nanofiber self-standing film with high volumetric and gravimetric capacitance performances for aqueous supercapacitors[J]. *Electrochimica Acta*, 2020, 337: 135800.
- [31] Chu M, Zhai Y, Shang N, N-doped carbon derived from the monomer of chitin for high-performance supercapacitor[J]. *Applied Surface Science*, 2020, 517: 146140.
- [32] Zhou Y, Yan W, Yu X, et al. Boron and nitrogen co-doped porous carbon for supercapacitors: A comparison between a microwave-assisted and a conventional hydrothermal process[J]. *Journal of Energy Storage*, 2020, 32: 101706.
- [33] Zhang W, Lin N, Liu D, et al. Direct carbonization of rice husk to prepare porous carbon for supercapacitor applications[J]. *Energy*, 2017, 128: 618-625.
- [34] Zhang Y, Shen Z, Yu Y, et al. Porous carbon derived from waste polystyrene foam for supercapacitor[J]. *Journal of Materials Science*, 2018, 53: 12115-12122.
- [35] Sun W, Lipka S, Swartz C, Hemp-derived activated carbons for supercapacitors[J]. *Carbon*, 2016, 103: 181-192.
- [36] Lu Q, Xu Y, Mu S, The effect of nitrogen and/or boron doping on the electrochemical performance of non-caking coal-derived activated carbons for use as supercapacitor electrodes[J]. *New Carbon Materials*, 2017, 32: 442-450.
- [37] Yu M, Han Y, Li J, et al. CO<sub>2</sub>-activated porous carbon derived from cattail biomass for removal of malachite green dye and application as supercapacitors[J]. *Chemical Engineering Journal*, 2017, 317: 493-502.

## Response surface optimization design and electrochemical performance of sword shell-based carbon

Luo Lu<sup>1</sup>, Deng Jianping<sup>1</sup>, Luo Lingcong<sup>1</sup>, Chen Tingting<sup>1</sup>, Fan Mizi<sup>1,2</sup>, Zhao Weigang<sup>1\*</sup>

(1. College of Material Engineering, Fujian Agriculture and Forestry University, Fuzhou 350018, Fujian, China; 2. College of Engineering, Design and Physical Sciences, Brunel University, Uxbridge UB8 3PH, London, United Kingdom)

**Abstract:** With the attention to the world ecology and economy, people are observing the abundant, low-cost, and clean renewable energy from sun and wind. However, most of the renewable energy sources are intermittent and cannot meet the needs for applications, except for converting to electricity. In order to satisfy the demand of people for new energy storage equipment, supercapacitors using biomass-based carbon materials as electrode materials have attracted much attention, because the multi-level structure of the natural biomass material is conducive to ion transmission. The fine structure of natural biomass cannot be synthesized artificially. The preservation of natural multi-scale structure can provide better electrochemical performance of the biomass-based carbon material. The biomass waste of sword beans shell with the characteristics of fast growth, a large amount of sword bean shells can be continuously produced as raw materials every year, but are often discarded or burned, which contributes to the environmental pollution. It is a promising precursor for obtaining hierarchically porous carbon-based material used as active component of high-storage capacity supercapacitors. The activated carbon with high surface area derived from sword shell by using KOH activation method and used as supercapacitor electrode materials. Taking the specific capacitance value of electrode material as the response value, the activation temperature and the activation ratio as the experimental factors, the Central Composite Design (CCD) method was employed to carry out the response surface optimization study, and the electrochemical performance of the activated carbon prepared under the optimal process conditions was explored. The research results show that the activation temperature and activation ratio have significant effects on the specific capacitance of activate carbon material. The coefficient  $R^2$  of the model is 97.54%, and the correction coefficient Adj  $R^2$  is 95.78%, indicating that the model can better predict the specific capacitance value of sword shell-based activated carbon with high reliability. The specific capacitance can reach a peak value under the condition of activation temperature 700 °C and the activation ratio 4 : 1. The optimized process parameters determined by center composite design approach were the activation temperature of 694 °C and the activation ratio of 4.17 : 1. The verification experiment shows that the average specific capacitance of the sword shell activated carbon material is 254 F/g, which is basically consistent with the predicted value. Furthermore, the Cyclic Voltammetry (CV) curves and Galvanostatic Charge-discharge (GCD) curves of different carbon materials were compared. A quasi-rectangular shape with wide hump peaks can be observed in CV curves, which can be attributed to the synergy between the Electric Double-layer Capacitance (EDLC) and the pseudocapacitance. The nitrogen fixation of legumes can provide carbon materials with nitrogen to produce redox reactions and provide pseudocapacitance. The GCD curves show nearly triangular shapes with a small deviation from linearity, which indicated excellent capacitive behavior of the electrode materials. The Nyquist plots from the Electrochemical Impedance Spectroscopy (EIS) analysis reveal that sword shell-based activated carbon has good electronic conductivity. Additionally, the physical properties of activated carbon was characterized. The apparent morphology of activated carbon was observed by Scanning Electron Microscope (SEM) and Transmission Electron Microscope (TEM). The nitrogen adsorption-desorption was conducted to investigate the pore structure of the carbon material. The results showed that: sword shell-based activated carbons possess a large number of nanopores, which distributed on the surface of the material, and the maximum specific surface area, total pore volume and micropore volume can up to 3 129 m<sup>2</sup>/g, 1.68 cm<sup>3</sup>/g and 0.96 cm<sup>3</sup>/g, which is conducive to electrolyte circulation and electrolyte ion adsorption.

**Keywords:** specific surface area; activated carbon; response surface; KOH activation; sword shells; supercapacitors